

Investigation of carbon fiber gas diffusion layers by means of synchrotron X-ray tomography

C. Tötze^{a,d}, I. Manke^a, C. Hartnig^{b,1}, R. Kuhn^b, H. Rieseemeier^c, J. Banhart^{a,d}

^a Helmholtz-Zentrum Berlin (HZB), 14109 Berlin, Germany

^b Zentrum für Sonnenenergie- und Wasserstoff-Forschung Baden-Württemberg (ZSW),
89081 Ulm, Germany

^c Bundesanstalt für Materialforschung und –prüfung, 12205 Berlin, Germany

^d Technische Universität Berlin, 10623 Berlin, Germany

¹ present address: Chemetall GmbH, Trakehner Straße 3, 60487 Frankfurt a. M.

The 3-dimensional spatial distribution of liquid water in different gas diffusion layer (GDL) materials was analyzed using synchrotron X-ray tomography. The capability of the method was demonstrated by virtually separating the GDL components in order to facilitate individual analysis of fiber material, liquid water and gas filled pore spaces.

The influence of hydrophobic surface treatment on the water distribution in the GDL was illustrated by analyzing three GDL materials with different degrees of hydrophobicity. In the least hydrophobic sample, liquid water tends to form larger clusters which stretch out about several hundred μm inside the porous GDL. In contrast, only small water clusters were found in the strongly hydrophobic material with high Polytetrafluoroethylene (PTFE)-content as the liquid is partially pressed out of the GDL. Additionally, the influence of fiber orientation on the water distribution in the felt material was demonstrated.

1. Introduction

Effective water management is a prerequisite for successful and reliable fuel cell operation. The gas diffusion layer (GDL) plays a key roll in water management: On one hand, a GDL is designed to prevent catalyst flooding by the rapid removal of excess liquid water from the active layer and the subsequent transfer to the flowfield channels. On the other hand, a GDL must maintain the level of membrane hydration necessary for proton conductivity.¹⁻³ Therefore, the characterization of liquid water distribution and transport dynamics of the GDL is an essential element for the enhancement of the water management.

Numerous theoretical⁴⁻⁸ and experimental⁹⁻¹⁰ studies focusing on two-phase flow in porous media contributed to the basic understanding of underlying water transport mechanisms. Recently, neutron and X-ray imaging were shown to be well suited for the investigation of water in porous materials like GDLs.^{7, 11-26} As neutron imaging offers large fields of view (typical size $10 \times 10 \text{ cm}^2$ as compared to only several mm^2 in the case of synchrotron X-ray imaging) this technique is especially capable of studying water distribution in larger samples, including complete fuel cells. Typical resolutions for such studies range from 20 to 100 μm . Synchrotron X-ray imaging, on the other hand, is the preferred method to investigate water distributions for smaller sample areas at higher

spatial resolution ($\sim 1 \mu\text{m}$) with typical image acquisition times of only few seconds. The application of synchrotron X-ray subsequent to neutron imaging can be a reasonable experimental strategy to explore interesting sample details, identified in the preceding neutron study, at higher spatial and temporal resolution.

Synchrotron X-ray imaging is generally applicable in the radiographic as well as in tomographic mode. Due to the short image acquisition time radiographic studies are able to analyze dynamic changes in the water distribution in fuel cells.^{20, 27} However, the method is limited to only two dimensions. In contrast, the tomographic mode allows for the analysis of the 3D spatial distribution of water for a static sample condition.^{25, 28} Furthermore, synchrotron X-ray tomography facilitates the three-dimensional examination of morphologic features relevant for transport in porous media samples.^{7, 18, 23, 28-29} Synchrotron X-ray tomography also has an essential advantages over common laboratory micro CT devices, i.e. the high photon flux typically between 10^{10} and $10^{12} \text{ mm}^{-2}\text{s}^{-1}$, which allows monochromatic measurements.

2. Experimental set-up

The experiments were performed at the Helmholtz-Zentrum Berlin using the synchrotron tomography station of the BAMline which is located at the synchrotron source BESSY (Berlin/Germany)³⁰. A W-Si monochromator with an energy resolution of $\Delta E/E=10^{-2}$ was used to obtain a monochromatic X-ray beam. The beam energy was adjusted to 13 keV in order to achieve optimal contrast between fibres, water and gas filled pore space.

Images were captured with a $2048 \times 2048 \text{ pixel}^2$ camera set-up (Princeton VersArray 2048B with a Gadox scintillator screen) rendering a field of view of up to $7 \times 7 \text{ mm}^2$ with pixel sizes of 1.5 and $3.5 \mu\text{m}$ and respective physical spatial resolutions of about 3 and $8 \mu\text{m}$.

Taking advantage of the monochromatic option the Circular GDL samples (type: Freudenberg H2315) with diameters of 3mm and 7mm were placed in a tubular sample holder and mounted on a translation/rotation unit. For each tomogram samples were rotated stepwise over an angular range of 180° . A radiographic set of 1800 projections were taken and, subsequently, reconstructed to a 3D volume. The exposure time for a single radiograph was 1s plus 4s read out time referring to a total acquisition time of 150 min for the complete tomographic scan.

3. Results and discussion

The first experiment demonstrates the feasibility of synchrotron X-ray tomography to visualize the 3D structure of microporous fiber-based GDL materials. Figure 1 shows details of the reconstructed sample volume of a dry sample. The felt type material consists of a porous network of carbon fibers with diameters about $10 \mu\text{m}$ which are mainly oriented in horizontal layers. Fibers are orientated rather randomly within these layers; however, sections also exist in which fibers run nearly parallel, forming bunches of a higher material concentration (see Figure 1 A+ B).

Figure 1 B and C demonstrate that the resolution is sufficient to resolve individual fibers. As a result, the tomographic data can be further exploited to determine morphological material parameters relevant for the transport properties, e.g. porosity and tortuosity of the material.³¹⁻³²

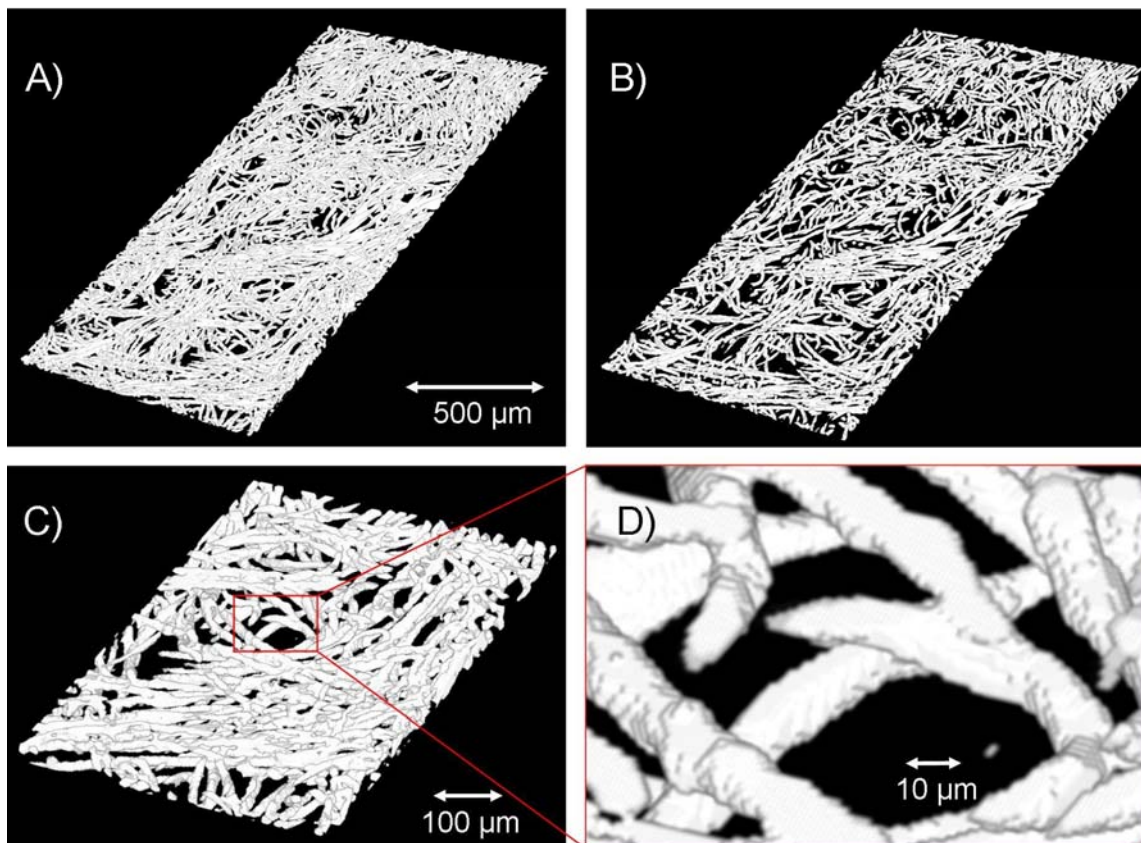


Figure 1. Details of the GDL sample revealing the 3D structure of the material. A) perspective view on a reconstructed volume (dimension $900 \times 1770 \times 26 \mu\text{m}^3$); B) perspective view on a horizontal layer (dimension $900 \times 1770 \times 14 \mu\text{m}^3$); C) perspective view on a selected detail (dimension $450 \times 525 \times 26 \mu\text{m}^3$); D) Magnified detail of C) demonstrating the capacity to resolve individual fibers

In the second set of experiments, tomograms were collected of water-saturated samples to study the 3D spatial distribution of the water in the GDL. To introduce water into the hydrophobic fiber structure, a stack of samples (of the same GDL specimens) was piled up in the sample holder. Subsequently, water was injected using a hypodermic needle. Figure 2 A, B, and C show GDL samples in the dry, a partially saturated and the saturated state, respectively. The fiber structure of the sample is readily identifiable in the dry sample (Figure 2 A). As observed in the first experiment, fibers are arranged in horizontal layers. Again, within the layers, fibers are orientated quite randomly, but a regular pattern of parallel streaks, i.e. areas of higher fiber concentration, can also be recognized. The streaks have some similarities in appearance and function with fabrics seams. They originate from a production step in which fibers are entangled in order to enhance cohesion between individual fiber layers. In contrast to the majority of fibers, entangled fibers also have an orientation component perpendicular to the layer orientation. Figure 2 B reveals the influence of the fiber entanglement on the water distribution. Owing to the hydrophobic nature of the material, a pressure gradient is necessary to push water into the porous material. The smaller the pores the more pressure is needed for water penetration. This explains the preferred water agglomeration in the area between the streaks, where pores are larger compared to those located in the regions of entanglement. As a result of the higher fiber concentration and the entailed smaller pore

diameters, the streaks are barriers for the lateral water transport. The streak pattern forms a template for water agglomerations stretching out in between adjacent streaks. The effect is even more pronounced at higher saturation (Figure 2 C) where extended water agglomerations form a structure of parallel, flooded channels. Only limited areas remain clear of water, forming a pattern of streaks.

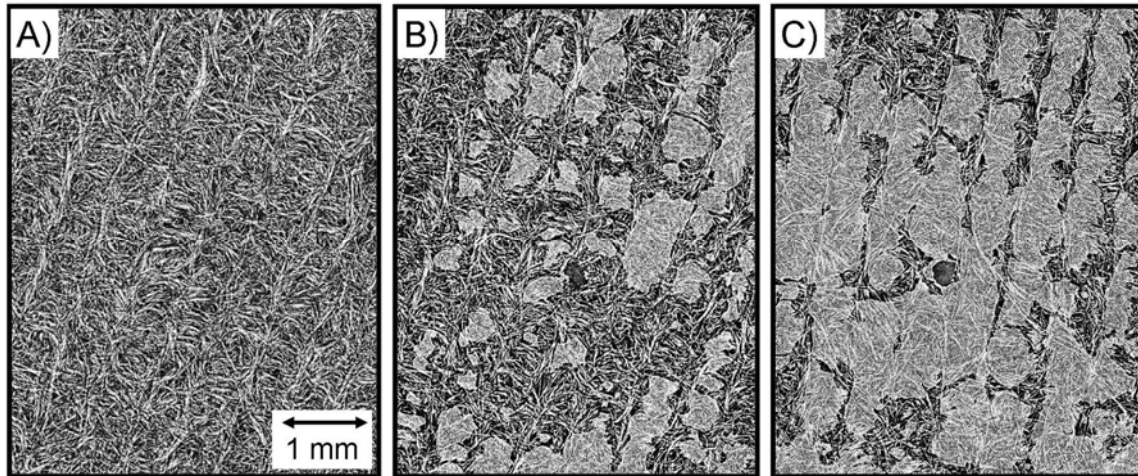


Figure 2. Cross section of hydrophilic GDL samples with a different degree of water saturation. A) dry sample; B) partially water filled; C) water saturated sample

Due to the different attenuation characteristics of the sample components, it is possible to virtually separate fibers, water and gas within the tomogram. To do so, the grey scale histogram is partitioned into an air, water and fiber subdivision by setting appropriate thresholds corresponding to the attenuation characteristics of the respective components as sketched in Figure 3.

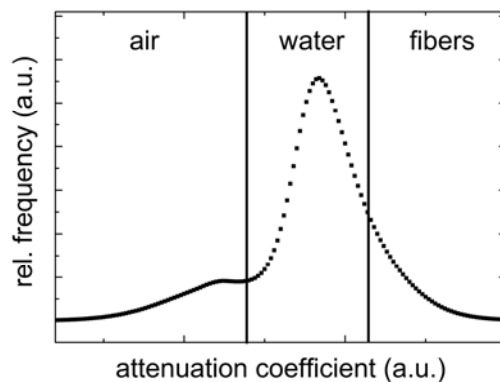


Figure 3: Grey scale histogram of the tomography of a water saturated GDL sample

The result is demonstrated in Figure 4 where the reconstructed volume of a GDL sample was split into the respective components using the software “VG Studio Max”. Individual components are depicted by adjusting the transparency of the subdivisions and by coloring the component to be highlighted. Figure 4 A shows a perspective view on a reconstructed sample volume. Individual false colors were assigned to the different components: fibers are colored in pink, water in blue, and gas filled pores in green.

Individual components can be easily analyzed when the remaining components are faded out. Figure 4 B shows the water distribution while in Figure 4 C the gas filled pores are highlighted. The analysis of individual distributions provides insights into the structural properties relevant for water transport in the GDL, e.g. porosity and tortuosity of the fiber material, fraction of unfilled pores, etc. The analysis of unfilled pores is of particular interest: Gas filled pores can serve as preferred transport paths for gas, however, isolated pores, i.e. pores completely bordered by water and fiber interfaces, do not contribute significantly to the media transport. This information is crucial for the understanding of the mass transport in the GDL and can be used as input data for water transport simulations or as validation basis for transport models.

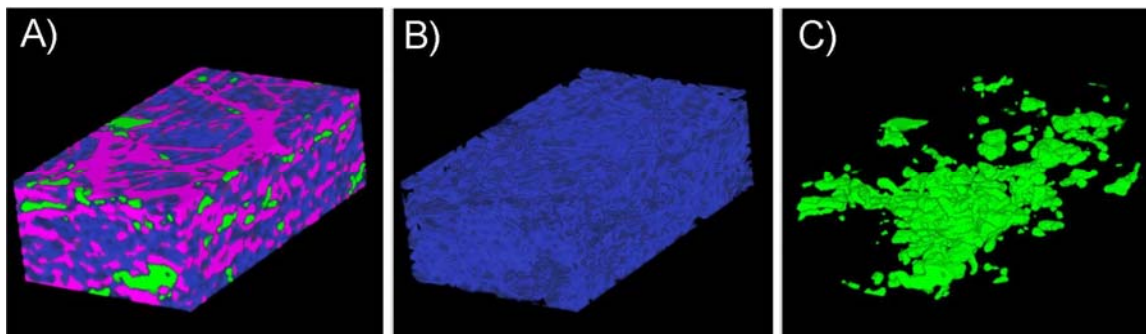


Figure 4. Phase separation in the reconstructed GDL volume using false colors. Water is shown in blue, fibers in pink, gas filled pores in green. A) representation of all 3 phases; B) water; C) gas filled pores³³

In a third set of experiments, the influence of hydrophobic surface properties of GDL-fibers on the water distribution was demonstrated. In order to achieve good water transport characteristics the degree of hydrophobicity of a GDL is adjusted during the production process. This is realized by a treatment with hydrophobic agents such as PTFE. To demonstrate the effect on the water management three samples containing different PTFE-loads (A: 0 wt.%, B: 12 wt.%, C: 30 wt.%) were saturated with water following the procedure described above and, subsequently, tomographies of these samples were performed. Representative cross sections of the samples are depicted in Figure 5. The effect of the PTFE treatment is obvious: the smaller the PTFE load, the larger the size of water agglomerates within the sample. In the untreated sample (Figure 5 A) water agglomerations extend to form connected structures with a size of about 1mm. When employed in a fuel cell these agglomerations can block complete gas channels in the flow field leading to undesired flooding effects and, consequently, to a performance drop of the cell. In contrast, only small water agglomerations can be found in the sample with the highest PTFE load (Figure 5 C) which indicates a very small intrusion rate. However, a water absorption capacity which is too low is also unfavorable. If too much PTFE is used in the hydrophobic treatment, the agent is not distributed uniformly throughout the whole GDL volumes but preferably agglomerates in the near surface regions forming a strong water barrier at the interface to the catalytic layer. The small intrusion rate and reduced water transport capacity may cause flooding effects in the catalyst layer during cell operation. An optimal hydrophobicity adjustment of the GDL aims at a water transport characteristic coping with the whole range of operational conditions, i.e. ensuring appropriate water evacuation from the catalyst layer as well as preventing flooding of flow field channels.

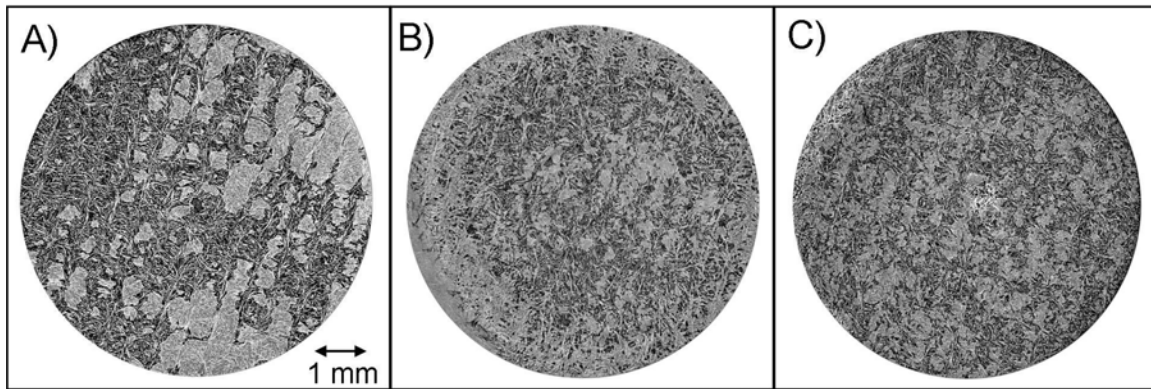


Figure 5. Water distribution in GDLs with different PTFE loads. A) 0 wt.% PTFE - low degree of hydrophobicity; B) 12 wt.% PTFE - intermediate degree of hydrophobicity; C) 30 wt.% PTFE - high degree of hydrophobicity

4. Conclusion/Outlook

Synchrotron tomography was demonstrated as powerful analyzing tool for water distributions in GDL materials. The detailed 3 dimensional visualization of the fiber network is used to extract morphologic information crucial for the understanding of media transport phenomena affecting the water management. The separation of the different phases present in the water saturated GDL facilitates the determination of important transport parameters like porosity, tortuosity or fraction of isolated pores. Prospective tomographic studies of the water distribution in GDLs will take account of more realistic operating conditions. This includes the non-uniform compression of the GDL by the flowfield meander, the establishment of a water pressure gradient in order to simulate a realistic water intrusion and an appropriate temperature conditioning of the GDL sample.

References

1. C.-Y. Wang, *Chemical Reviews* **104** (10), 4727-4766 (2004).
2. W. Vielstich, A. Lamm and H. A. Gasteiger, (John Wiley & Sons, Chichester, 2003), Vol. 3.
3. L. Carrette, K. A. Friedrich and U. Stimming, *Fuel Cells* **1** (1), 5-39 (2001).
4. U. Pasaogullari and C.-Y. Wang, *Journal of The Electrochemical Society* **152** (2), A380-A390 (2005).
5. C. Ziegler, H. M. Yu and J. O. Schumacher, *Journal of The Electrochemical Society* **152** (8), A1555-A1567 (2005).
6. C. Y. Wang and P. Cheng, *International Journal of Heat and Mass Transfer* **39** (17), 3607-3618 (1996).
7. P. K. Sinha, P. P. Mukherjee and C. Y. Wang, *Journal of Materials Chemistry* **17**, 3089-3103 (2007).
8. P. Zhou and C. W. Wu, *Journal of Power Sources* **195**, 1408-1415 (2010).
9. A. Bazylak, D. Sinton and N. Djilali, *Journal of Power Sources* **176** (1), 240-246 (2008).
10. S. Litster, D. Sinton and N. Djilali, *Journal of Power Sources* **154** (1), 95-105 (2006).
11. R. J. Bellows, M. Y. Lin, M. Arif, A. K. Thompson and D. Jacobson, *Journal of The Electrochemical Society* **146** (3), 1099-1103 (1999).
12. R. Satija, D. L. Jacobson, M. Arif and S. A. Werner, *Journal of Power Sources* **129** (2), 238-245 (2004).
13. M. A. Hickner, N. P. Siegel, K. S. Chen, D. S. Hussey, D. L. Jacobson and M. Arif, *Journal of The Electrochemical Society* **155** (4), B427-B434 (2008).
14. A. B. Geiger, A. Tsukada, E. Lehmann, P. Vontobel, A. Wokaun and G. G. Scherer, *Fuel Cells* **2** (2), 92-98 (2002).
15. P. Boillat, G. Frei, E. H. Lehmann, G. G. Scherer and A. Wokaun, *Electrochemical and Solid-State Letters* **13** (3), B25-B27 (2010).
16. M. Strobl, I. Manke, N. Kardjilov, A. Hilger, M. Dawson and J. Banhart, *Journal of Physics D-Applied Physics* **42** (24) (2009).
17. N. Pekula, K. Heller, P. A. Chuang, A. Turhan, M. M. Mench, J. S. Brenizer and K. Ünlü, *Nuclear Instruments and Methods in Physics Research Section A: Accelerators, Spectrometers, Detectors and Associated Equipment* **542** (1-3), 134-141 (2005).
18. P. K. Sinha, P. Halleck and C.-Y. Wang, *Electrochemical and Solid-State Letters* **9** (7), A344-A348 (2006).
19. I. Manke, C. Hartnig, N. Kardjilov, H. Riesemeier, J. Goebbels, R. Kuhn, P. Krüger and J. Banhart, *Fuel Cells* **10** (1), 26-34 (2010).
20. I. Manke, C. Hartnig, M. Grunerbel, W. Lehnert, N. Kardjilov, A. Haibel, A. Hilger, J. Banhart and H. Riesemeier, *Applied Physics Letters* **90** (17), 174105 (2007).
21. C. Hartnig, I. Manke, J. Schloesser, P. Krüger, R. Kuhn, H. Riesemeier, K. Wippermann and J. Banhart, *Electrochemistry Communications* **11** (8), 1559-1562 (2009).

22. J. Banhart, A. Borbely, K. Dzieciol, F. Garcia-Moreno, I. Manke, N. Kardjilov, A. R. Kaysser-Pyzalla, M. Strobl and W. Treimer, *International Journal of Materials Research* **101** (9), 1069-1079 (2010).
23. S. R. Stock, *International Materials Reviews* **53**, 129-181 (2008).
24. N. Kardjilov, I. Manke, A. Hilger, M. Strobl and J. Banhart, *Materials Today* **14** (6), 248-256 (2011).
25. P. Krüger, H. Markötter, J. Haußmann, M. Klages, T. Arlt, J. Banhart, C. Hartnig, I. Manke and J. Scholta, *Journal of Power Sources* **196** (12), 5250-5255 (2011).
26. A. Schröder, K. Wippermann, J. Mergel, W. Lehnert, D. Stolten, T. Sanders, T. Baumhöfer, D. U. Sauer, I. Manke, N. Kardjilov, A. Hilger, J. Schloesser, J. Banhart and C. Hartnig, *Electrochemistry Communications* **11** (8), 1606-1609 (2009).
27. C. Hartnig, I. Manke, R. Kuhn, S. Kleinau, J. Goebbels and J. Banhart, *Journal of Power Sources* **188** (2), 468-474 (2009).
28. H. Markötter, I. Manke, P. Krüger, J. Haußmann, M. Klages, T. Arlt, H. Rieseemeier, C. Hartnig, J. Scholta and J. Banhart, *Electrochemistry Communications* (2011 (accepted DOI 10.1016/j.elecom.2011.06.023)).
29. J. Banhart, (Oxford University Press, Oxford, UK, 2008).
30. W. Görner, M. P. Hentschel, B. R. Müller, H. Rieseemeier, M. Krumrey, G. Ulm, W. Diete, U. Klein and R. Frahm, *Nuclear Instruments and Methods in Physics Research Section A: Accelerators, Spectrometers, Detectors and Associated Equipment* **467-468** (Part 1), 703-706 (2001).
31. R. Thiedmann, C. Hartnig, I. Manke, V. Schmidt and W. Lehnert, *Journal of the Electrochemical Society* **156** (11), B1339-B1347 (2009).
32. I. Manke, H. Markötter, C. Tötzke, N. Kardjilov, R. Grothausmann, M. Dawson, C. Hartnig, S. Haas, D. Thomas, A. Hoell, C. Genzel and J. Banhart, *Advanced Engineering Materials* **DOI: 10.1002/adem.201000284** (2011).
33. C. Hartnig, R. Kuhn, P. Kruger, I. Manke, N. Kardjilov, J. Goebbels, B. R. Muller and H. Rieseemeier, *Materials Testing-Materials and Components Technology and Application* **50** (10), 609-614 (2008).